Article

Attaining Control by Design over the Hydrolytic Stability of Fe-TAML Oxidation Catalysts

Victor Polshin, Delia-Laura Popescu, Andreas Fischer, Arani Chanda, David C. Horner, Evan S. Beach, Jennifer Henry, Yong-Li Qian, Colin P. Horwitz, Gabor Lente, Istvan Fabian, Eckard Mnck, Emile L. Bominaar, Alexander D. Ryabov, and Terrence J. Collins

J. Am. Chem. Soc., **2008**, 130 (13), 4497-4506 • DOI: 10.1021/ja7106383

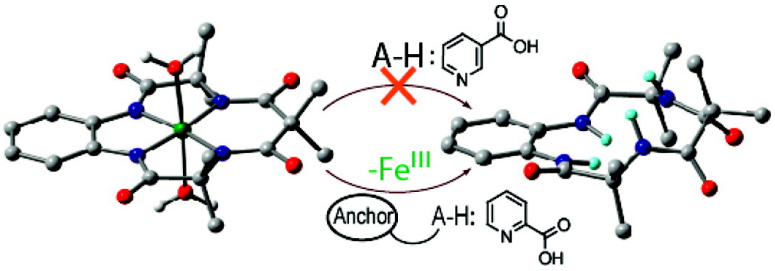

More About This Article

Additional resources and features associated with this article are available within the HTML version:

- Supporting Information
- Links to the 1 articles that cite this article, as of the time of this article download
- Access to high resolution figures
- Links to articles and content related to this article
- Copyright permission to reproduce figures and/or text from this article

View the Full Text HTML

J|A|C|S
ARTICLES
Published on Web 03/12/2008

Attaining Control by Design over the Hydrolytic Stability of Fe-TAML Oxidation Catalysts

Victor Polshin,[†] Delia-Laura Popescu,[†] Andreas Fischer,[‡] Arani Chanda,[†] David C. Horner,[†] Evan S. Beach,[†] Jennifer Henry,[†] Yong-Li Qian,[†] Colin P. Horwitz,[†] Gabor Lente,[§] Istvan Fabian,[§] Eckard Münck,[†] Emile L. Bominaar,[†] Alexander D. Ryabov,*[,†] and Terrence J. Collins*[,†]

Department of Chemistry, Carnegie Mellon University, 4400 Fifth Avenue, Pittsburgh, Pennsylvania 15213, Inorganic Chemistry, Department of Chemistry, Royal Institute of Technology, S-100 44 Stockholm, Sweden, and Department of Inorganic and Analytical Chemistry, University of Debrecen, Debrecen, Hungary

Received December 5, 2007; E-mail: ryabov@andrew.cmu.edu; tc1u@andrew.cmu.edu

Abstract: The iron(III) complexes of tetra amidato macrocyclic ligands (TAMLs) ([Fe{1-X_1-2-$X_2C_6H_2$-4,5-$(NCOCMe_2NCO)_2CR_2$}(OH_2)]$^-$, **1**: $X_1 = X_2 = H$, $R_2 = Me_2$ (**a**), $R_2 = (CH_2)_2$ (**b**); $X_1 = X_2 = Cl$, $R_2 = F_2$ (**c**), etc.), which the proton is known to demetalate at pH < 3, are also subject to catalyzed demetalation by Brønsted acid buffer components at pH 4−9 such as $H_2PO_4^-$, HSO_3^-, and CH_3CO_2H, $HO_2CCH_2CO_2^-$. Buffers based on pyridine (py) and tris(hydroxymethyl)aminomethane (TRIS) are catalytically inactive. Where reactions proceed, the products are demetalated TAMLs and iron species of variable composition. Pseudo-first-order rate constants for the demetalation (k_{obs}) are linear functions of the acid concentrations, and the effective second-order rate constants $k_{1,eff}$ have a hyperbolic dependence on $[H^+]$ ($k_{1,eff} = a_1[H^+]/(b_1+[H^+])$. The rate of demetalation of **1a** in $H_2PO_4^-/HPO_4^{2-}$ buffer is appreciable, but the k_{obs} values for **1b** and **1c** are immeasurably low, showing that the rates are strongly affected by the CR_2 or "tail" fragments, which are known to potently affect the TAML basicity. The reactivities of **1** depend insignificantly on the aromatic ring or "head" group of **1**. The proposed mechanism involves precoordination of the acidic buffer species followed by hydrolysis. The demetalating abilities of buffer species depend on their structures and acidities. Thus, although pyridine-2-carboxylic (picolinic) acid catalyzes the demetalation, its 3- and 4-isomers (nicotinic and isonicotininc acids) are inactive. The difference is rationalized to result from the ability that only coordinated picolinic acid has to deliver a proton to an amidato nitrogen in an intramolecular manner. The reaction order in picolinic acid equals one for **1a** and two for **1b**. For **1b**, "inactive" pyridine and nicotinic acid speed up the demetalation in the presence of picolinic acid, suggesting that the second order arises from the axial binding of two pyridine molecules, one of which must be picolinic acid. The binding of pyridine- and imidazole-type ligands was confirmed by UV/vis equilibrium measurements and X-ray crystallography. The implications of these mechanistic findings for designing superior Fe-TAML oxidation catalysts and catalyst formulations are discussed using the results of DFT calculations.

Introduction

Iron(III) tetra amidato macrocyclic ligand (TAML) activators of the type shown in Chart 1 are exceptionally active catalysts for a variety of oxidations by hydrogen peroxide and organic peroxides in aqueous solutions.[1−7] The catalytic activity of **1** is comparable to that of enzymes utilizing H_2O_2 as a source of oxidation equivalents.[7,8] The activities are also strongly pH-dependent. Therefore, understanding the interactions of the catalysts with the components of reaction media that control acidity, ionic strength and ionic composition to impact the solution stability of Fe^{III}-TAMLs is critical for improving their performance by iterative design.[1,9] Such understanding is also fundamental to optimizing the formulation of reactive preparations and stock catalyst solutions and for finding the most favorable conditions for their long-term storage in solution.

[†] Carnegie Mellon University.
[‡] Royal Institute of Technology.
[§] University of Debrecen.

(1) Collins, T. J. *Acc. Chem. Res.* **2002**, *35*, 782−790.
(2) Sen Gupta, S.; Stadler, M.; Noser, C. A.; Ghosh, A.; Steinhoff, B.; Lenoir, D.; Horwitz, C. P.; Schramm, K.-W.; Collins, T. J. *Science* **2002**, *296*, 326−328.
(3) Banerjee, D.; Markley, A. L.; Yano, T.; Ghosh, A.; Berget, P. B.; Minkley, E. G., Jr.; Khetan, S. K.; Collins, T. J. *Angew. Chem., Int. Ed.* **2006**, *45*, 3974−3977.
(4) Horwitz, C. P.; Collins, T. J.; Spatz, J.; Smith, H. J.; Wright, L. J.; Stuthridge, T. R.; Wingate, K. G.; McGrouther, K. *ACS Symp. Ser.* **2006**, *921*, 156−169.
(5) Mondal, S.; Hangun-Balkir, Y.; Alexandrova, L.; Link, D.; Howard, B.; Zandhuis, P.; Cugini, A.; Horwitz, C. P.; Collins, T. J. *Catal. Today* **2006**, *116*, 554−561.
(6) Chanda, A.; Khetan, S. K.; Banerjee, D.; Ghosh, A.; Collins, T. J. *J. Am. Chem. Soc.* **2006**, *128*, 12058−12059.
(7) Chahbane, N.; Popescu, D.-L.; Mitchell, D. A.; Chanda, A.; Lenoir, D.; Ryabov, A. D.; Schramm, K.-W.; Collins, T. J. *Green Chem.* **2007**, *9*, 49−57.
(8) Ghosh, A.; Mitchell, D. A.; Chanda, A.; Ryabov, A. D.; Popescu, D. L.; Upham, E.; Collins, T. J. Manuscript in preparation, 2008.

Chart 1. Iron(III)-TAML Activators Used in This Work

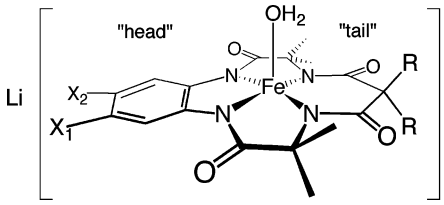

1	X_1	X_2	R
a	H	H	Me
b	H	H	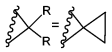
c	Cl	Cl	F
d	Me	Me	Me
e	Cl	Cl	Me
f	MeO	MeO	Me

During the course of the Fe^{III}-TAML design and development work, we have found that the **1** complexes are stable for weeks in non-buffered HPLC-grade water, but only for days in a dilute (~0.01 M) phosphate buffer at pH 7. At [phosphate] ≫ 0.01 M, **1a** degrades at pH 7−8. These and related findings were perplexing and signaled that there might be unexpected constraints on the utility of Fe^{III}-TAMLs in real-world processes. Since it is often important to conduct Fe^{III}-TAML-catalyzed processes in buffered solutions, we embarked on extended studies to determine the mechanistic characteristics giving rise to the newfound solution instabilities. In a general sense, the cleavage of the Fe−N bonds are hydrolysis reactions that may be catalyzed either by the aquated proton (specific acid catalysis) or by all sources of protons in the solution with each source contributing to enhancing the rate and with the stronger acids being more effective (general acid catalysis).[10] The two catalysis types are usually differentiated by determining the rate dependence on the buffer concentration while keeping the pH constant. A constant rate provides evidence for specific acid catalysis. A buffer dependent rate signals the process is under general acid catalysis. In our prior report, the demetalation processes were found to be subject to specific acid catalysis.[19] However, as we show here, particular buffering agents can also cause demetalation outside the specific acid catalysis region under considerably more basic conditions. We will also show furthermore that the hydrolysis reactions are not typical examples of general acid catalysis, because they occur only when a Brønsted acid can precoordinate to the iron and has an appropriate structure for intramolecular delivery of a proton to a coordinated amido nitrogen. The results reported here establish the origin of the instabilities and are organized around the following topics: (i) a mechanistic analysis of the demetalation of **1** by common buffer components such as phosphate in slightly acidic to neutral aqueous solutions; (ii) the unusual demetalation of **1** by pyridine-2-carboxylic acid, which follows either first or second-order kinetics depending on the nature of **1**; (iii) the quantitative description with X-ray characterization of the equilibrium binding to **1** of nitrogen donor ligands such as pyridine, imidazole, and azide; (iv) the proposal of a general mechanism of the buffer-induced demetalations based on experimental data and supported by DFT calculations. As the study shows, by discovering likely mechanisms of these novel buffer-ion promoted demetalations, one can completely avoid them either by designing the Fe^{III}-TAML to resist the degradations or by setting the process or solution storage conditions so that vulnerable catalysts are not degraded.

Results and Discussion

Catalyzed Demetalation of 1 in Phosphate Buffer. The tetra-deprotonated macrocyclic ligands in **1** are arranged in a distorted planar conformation around Fe^{III} in the solid state, as determined by a number of crystal structures.[19−21] The free ligand itself is nonplanar.[20] The central metal in **1** and in other transition metal TAML complexes[9] induce ligand conformations required for mononuclear complexes. For each complex, the cleavage of a single Fe−N linkage in water leads to rapid hydrolysis of the remaining bonds and liberation of the free TAML ligand.[19] The *proton*-induced demetalation of **1** is known to follow a two-term rate law with $k_{obs} = k_1[H^+] + k_3[H^+]^3$ at pH < 3.[19] The iterative design of the TAML system[9] has produced catalysts with enhanced resistance toward the free proton that ranges over five and eleven orders of magnitude in terms of k_1 and k_3, respectively.[19] However, when phosphate concentrations of >0.1 M are used for adjusting the pH of solutions of **1a**, the release of iron(III) can be observed visually *via* the fading of the complex's orange color. Remarkably, the demetalation occurs even around pH 7 under ambient temperature where **1a** is stable at neutral pH in unbuffered water for periods of months. When the decomposition is monitored by UV/vis spectroscopy, the principal band of **1a** at 368 nm diminishes gradually with time (Figure 1) and a white precipitate forms. This precipitate was shown by ^{1}H NMR analysis in CD_3-OD to be the free TAML, which was first collected by filtration after running the demetalation at 0.08 M **1a** in 0.5 M phosphate at pH 7 for 12 h; the aromatic AA'BB' signals were found at δ 7.50 and 7.35 with the methyl signals at the expected locations of δ 1.593 and 1.586—the amide N−H protons were not observed as they exchange with deuterium in methanol-d_4.

The tail portion of the macrocyclic ligand significantly influences the reactivity of Fe^{III}-TAML complexes toward this buffer-induced demetalation. The inset to Figure 1 compares the dimethyl- (**1a**), cyclopropyl- (**1b**), and difluoro-tailed (**1c**)

(9) Collins, T. J. *Acc. Chem. Res.* **1994**, *27*, 279−285.
(10) General acid catalysis has been encountered but is still rather unexplored for transition metal complexes. The reported examples include, for example, amine and amide complexes of nickel(II),[11−13] peptide copper(II) species,[14] Cu^{II} and Pb^{II} complexes of diazapolyoxa-*N*,*N*′-diacetic acids,[15] calcium and lithium cryptates,[16−17] and macrocyclic complexes of Co^{II}.[18]
(11) Paniago, E. B.; Margerum, D. W. *J. Am. Chem. Soc.* **1972**, *94*, 6704−6710.
(12) Read, R. A.; Margerum, D. W. *Inorg. Chem.* **1981**, *20*, 3143−3149.
(13) Read, R. A.; Margerum, D. W. *Inorg. Chem.* **1983**, *22*, 3447−3451.
(14) Wong, L. F.; Cooper, J. C.; Margerum, D. W. *J. Am. Chem. Soc.* **1976**, *98*, 7268−7274.
(15) Laing, J. L.; Taylor, R. W.; Chang, C. A. *J. Chem. Soc., Dalton Trans.* **1997**, 1195−1200.
(16) Cox, B. G.; Schneider, H. *J. Am. Chem. Soc.* **1980**, *102*, 3628−3630.
(17) Cox, B. G.; Jedral, W.; Firman, P.; Schneider, H. *J. Chem. Soc., Perkin Trans. 2* **1981**, 1486−1491.
(18) Gazzaz, H. A.; El-Guindi, N. M.; El-Awady, A. A. *J. Chem. Soc., Dalton Trans.* **1993**, 2313−2320.
(19) Ghosh, A.; Ryabov, A. D.; Mayer, S. M.; Horner, D. C.; Prasuhn, D. E., Jr.; Sen Gupta, S.; Vuocolo, L.; Culver, C.; Hendrich, M. P.; Rickard, C. E. F.; Norman, R. E.; Horwitz, C. P.; Collins, T. J. *J. Am. Chem. Soc.* **2003**, *125*, 12378−12378.
(20) Bartos, M. J.; Gordon-Wylie, S. W.; Fox, B. G.; Wright, L. J.; Weintraub, S. T.; Kauffmann, K. E.; Münck, E.; Kostka, K. L.; Uffelman, E. S.; Rickard, C. E. F.; Noon, K. R.; Collins, T. J. *Coord. Chem. Rev.* **1998**, *174*, 361−390.
(21) Chanda, A.; Popescu, D.-L.; Tiago, de Oliveira, F.; Bominaar, E. L.; Ryabov, A. D.; Muenck, E.; Collins, T. J. *J. Inorg. Biochem.* **2006**, *100*, 606−619.

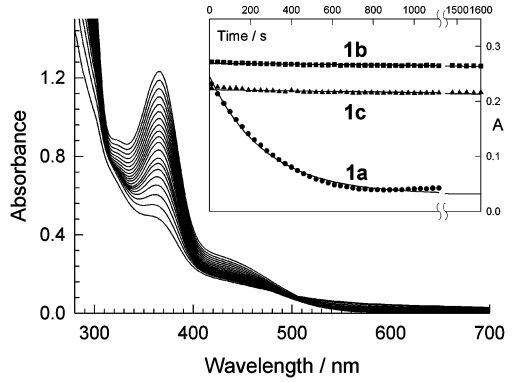

Figure 1. Spectral changes of **1a** (2.5×10^{-4} M) in 0.2 M phosphate buffer (pH 7.3, 25 °C) registered within 18 h time period. (Inset) Dynamics of demetalation of **1a**, **1b**, and **1c** in 0.5 M phosphate buffer solution at pH 6.0 and 65 °C.

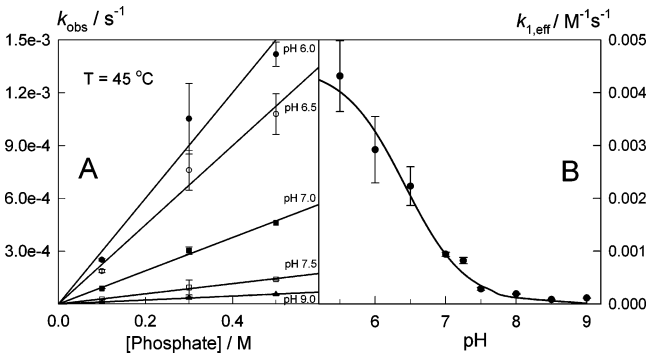

Figure 2. (A) Pseudo-first-order rate constants for demetalation of **1a** *versus* phosphate concentration at different pHs and 45 °C. (B) Second-order rate constants $k_{1,eff}$ for demetalation of **1a** as a function of pH at 45 °C. Solid line is a theoretical curve calculated using the best-fit values of parameters of eq 1.

complexes under identical reaction conditions. Compounds **1b** and **1c** undergo essentially no change in 30 min while **1a** is demetalated in less than 15 min. This could be taken to suggest an obvious line of research to solve the buffer-induced stability problem—**1a** should not be used in processes involving phosphate buffers, but rather only **1b** and **1c** should be investigated for such. However, from both green chemistry and practical perspectives, **1a** looks more attractive than **1b** or **1c**. Unlike **1c**, **1a** is halogen-free and therefore one can surmise that it will be less likely to lead to persistent degradation fragments that in turn could lead to unanticipated toxicities. The cyclopropyl group of **1b** is also a somewhat rare biological functionality and more suspect of unanticipated toxicity than the dimethyl tail of **1a**. Also both the difluoro and cyclopropyl fragments of **1b** and **1c** seem certain to add to the costs of the catalyst compared with **1a**. Thus, we needed to fully understand the demetalation with the hope of establishing **1a** as a viable catalyst for applications and even for longterm storage in buffered solutions.

Data such as those in Figure 1 do not allow for reliable measurement of k_{obs} for the much less reactive catalysts, **1b** and **1c**, without moving to more acidic conditions. Unfortunately, with the lowering of pH the proton driven demetalation begins to dominate. Therefore **1a** was used for collecting kinetic data (35−65 °C).[22] Pseudo-first-order rate constants for the decay of **1a** (k_{obs}) are directly proportional to the phosphate concentration without a noticeable intercept. Phosphate-independent demetalation is thus negligible here (Figure 2A). The effective second-order rate constants $k_{1,eff}$ (subscript 1 denotes first order in acid) calculated from the slopes of linear plots are shown as a function of pH in Figure 2B. Thus, k_{obs} increases with increasing [phosphate] at constant pH and the effect is stronger at lower pH (Figure 2A).[23] The sigmoid profile of $k_{1,eff}$ in Figure 2B, with its right part approaching zero with an inflection point at ∼6.5, co-incident with the pK_a of dihydrogen phosphate, implicates $H_2PO_4^-$ as a major participant in the demetalation.

$$k_{1,eff} = \frac{a_1[H^+]}{b_1 + [H^+]} \qquad (1)$$

The data in Figure 2B was quantified in terms of eq 1 that agrees with a mechanism shown in Scheme 1. It will be shown below (see eq 10) that $a_1 = K_{LH}k_{ML}$ and $b_1 = K_{a2}$. The best-fit values for a_1 and b_1 obtained at four temperatures are summarized in

Scheme 1. Tentative Mechanism for the Phosphate-Induced Demetalation of Fe^{III}-TAMLs

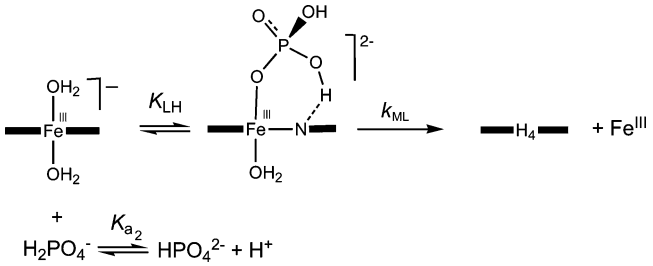

Table 1. The rate and equilibrium constants at 45 °C were used to calculate a theoretical solid line in Figure 2B.

The rate-limiting step of the mechanism in Scheme 1 is intramolecular in nature. While it is possible that $H_2PO_4^-$ could attack **1** from the bulk solution in a kinetically indistinguishable manner, more likely the process proceeds as suggested in Scheme 1 through pre-equilibrium binding of $H_2PO_4^-$. We favor this explanation especially because pyridine-2-carboxylic (picolinic) acid catalyzes the demetalation, whereas its 3- and 4-structural isomers do not. Coordinated picolinic acid is sterically able to deliver a proton to an amido-N atom in an intramolecular fashion, whereas the 3- and 4-structural isomers are not so able (see below). We postulate that the binding of $H_2PO_4^-$ to the Fe^{III}-TAML is followed by the slow intramolecular delivery of a proton to one Fe−N bond, resulting in its cleavage, followed by fast protonolyses/hydrolyses of the remaining Fe−N bonds in a related manner to the mechanistic features used to explain the data on the demetalation of Fe^{III}-TAMLs by H^+.[19]

Despite the mechanistic explanation of Scheme 1, we have not found direct evidence for a strong binding of dihydrogenphosphate to **1**. Rather, several lines of evidence support weak phosphate binding. (i) The k_{obs} does not level off at high phosphate concentrations. (ii) The λ_{max} in the UV/vis spectrum of **1b** does not change its position in the presence of 0.01, 0.3, and 0.5 M phosphate at pH 7.5 (Figure 3) and the absorbance intensity varies negligibly.

(22) Catalyst **1a** has been produced in >100 kg and is moving to multitonne production. Thus, at this stage of the development of Fe-TAML activators for green applications, it is most important to optimize the performance of **1a**.
(23) These features indicate a general acid mechanism of the demetalation.[24,25]
(24) Jencks, W. P. *Catalysis in Chemistry and Enzymology*; McGraw-Hill Book Company: New York, 1969.
(25) Espenson, J. H. *Chemical Kinetics and Reaction Mechanisms*, 2nd ed.; McGraw-Hill, Inc.: New York, 1995.

Table 1. Parameters of eq 1, Values of pK_a, Activation, and Thermodynamic Parameters for the Demetalation of **1**

TAML	catalyst	T/°C	a_1/M^{-1} s^{-1}	b_1 (K_a)/M	pK_a	lit pK_a [38a]
1a	$H_2PO_4^-$	35	$(2.68 \pm 0.03) \times 10^{-3}$	$(5.2 \pm 0.2) \times 10^{-7}$	6.29 ± 0.02	6.57 ± 0.05
		45	$(4.5 \pm 0.3) \times 10^{-3}$[b]	$(3.8 \pm 0.7) \times 10^{-7}$	6.42 ± 0.09	
		55	$(7.8 \pm 0.3) \times 10^{-3}$	$(12 \pm 1) \times 10^{-7}$	5.92 ± 0.05	
		65	$(14.9 \pm 0.5) \times 10^{-3}$	$(11.0 \pm 0.8) \times 10^{-7}$	5.96 ± 0.03	
1a	HSO_3^-	65	$(6 \pm 2) \times 10^{-2}$	$(8 \pm 5) \times 10^{-6}$	5.1 ± 0.6	6.0[c]
1a	CH_3COOH	65	0.13 ± 0.02	$(6 \pm 1) \times 10^{-4}$	3.3 ± 0.1[d]	4.56 ± 0.03
1a	$H_2C(COOH)_2$	65	0.19 ± 0.02	$(4 \pm 1) \times 10^{-5}$	4.5 ± 0.2	5.07 ± 0.06
						2.57 ± 0.05
1a	Me_3CCOOH	65	no catalysis			4.83 ± 0.01
1a	Pyridine	65	no catalysis			5.229
1a	Picolinic acid (P2C)	25	0.46 ± 0.07	$(3 \pm 1) \times 10^{-5}$	4.5 ± 0.2	5.17 ± 0.01
1d	Picolinic acid (P2C)	25	0.34 ± 0.04	$(2.6 \pm 0.8) \times 10^{-5}$	4.6 ± 0.1	
1e	Picolinic acid (P2C)	25	0.20 ± 0.01	$(1.5 \pm 0.3) \times 10^{-5}$	4.83 ± 0.06	
1b	Picolinic acid (P2C)	65	0.116 ± 0.007[e]	$(1.5 \pm 0.3) \times 10^{-5}$	4.9 ± 0.1	
						0.86 ± 0.02
1a	Nicotinic acid (P3C)	65	no catalysis			4.81 ± 0.03
						2.05 ± 0.03
1a	Isonicotinic acid (P4C)	65	no catalysis			4.87 ± 0.04
						1.79 ± 0.04
1a	$(HOCH_2)_3CNH_2$ (TRIS)	65	no catalysis			8.075
1a	HN_3	25	no catalysis			4.65 ± 0.02

[a] Summarized for general reference the values in this column are at 25 °C predominantly at 0−0.1 M ionic strength. [b] $\Delta H^{\neq} = 47 \pm 5$ kJ mol^{-1}, $\Delta S^{\neq} = -143 \pm 2$ J mol^{-1} K^{-1}. [c] Extrapolated to 65 °C using the value of 6.36 at 25 °C and $\Delta H°$ of 12.6 kJ mol^{-1}.[38] An effect of phosphate on lowering pK_a cannot be excluded. [d] Observed low experimental pK_a value for acetate presumably results from interference from specific acid catalysis at higher acidities. [e] In M^{-2} s^{-1}.

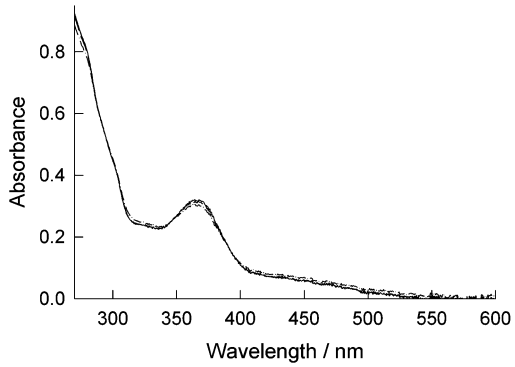

Figure 3. Spectra of **1b** in the presence of 0.01 (solid), 0.3 (dash), and 0.50 (dash-dot) M phosphate concentrations at pH 7.5 and 25 °C when the demetalation is immeasurably slow.

Other potential acids that could give rise to a similar $H_2PO_4^-$ effect have been tested including hydrogen sulfite, acetic acid, and tris(hydroxymethyl)aminomethane [$(HOCH_2)_3CNH_2$·HCl, TRIS]. The effect of sulfite toward **1a** was studied in the range 0.1−0.5 M at pH 5.25−6.75 and 65 °C. Sulfite is a poor buffer and therefore the solution pH was maintained by adding 0.1 M phosphate buffer. Plots of k_{obs} *versus* concentration of added sulfite were linear with nonzero intercepts attributable to the constant $H_2PO_4^-$ contribution. A graph similar to the one in Figure 2A was generated by plotting $k_{1,eff}$ (the slopes) against pH (see Supporting Information (SI), Figure 1S). A fit of the kinetic data to eq 1 gave parameters a_1 and b_1 (Table 1). Similar behavior was found for acetic and malonic acids (see Supporting Information, Figures 2S and 3S, respectively); parameters a_1 and b_1, calculated as above, are shown in Table 1. There is a Brønsted correlation between log a_1 (log $K_{LH}k_{ML}$) and $-\log b_1$ (pK_a) with the slope *ca.* −0.3, i.e., the activity of the acids increases with increasing acidity (Figure 4S, Supporting Information). This is a typical property of reactions proceeding *via* a general acid mechanism, although one could argue that the present coordination/protonolysis process is not a true general acid catalysis. Notably, TRIS (pK_a = 7.83 for protonated amine[26]) does not demetalate **1a**, even if the pH is lowered to 4.5 and the solution is heated to 65 °C for 1 h. While the amine is a likely coordinating group, upon its coordination the only groups that can deliver a proton in an intramolecular fashion to the effect amidato protonolysis are the primary alcohols. However, compared with $H_2PO_4^-$ and HSO_3^-, the alcohol groups have a considerably higher pK_a value and these are apparently not acidic enough to initiate the demetalation. Thus, it becomes clear that it is indeed possible to use **1a** in a buffered solution providing that the buffering ion, if it can coordinate to the iron, cannot participate in a favorable intramolecular delivery of a proton to a coordinated amide group.

Demetalation by Pyridine-X-Carboxylic Acids {PXC, X = 2 (Picolinic), 3 (Nicotinic), and 4 (Iso-nicotinic)}. An intriguing differential activity of pyridine carboxylic acids in the demetalation of **1** was discovered that is strongly suggestive of the proposed buffer coordination/protonolysis mechanism. Pyridine, nicotinic and isonicotinic acids by themselves are inactive under a wide range of reaction conditions. In contrast, picolinic acid demetalates complex **1a** at 25 °C showing behavior similar to that described for phosphate and sulfite (Figure 4), *i.e.*, k_{obs} increases linearly with increasing picolinic acid concentration and the slopes ($k_{1,eff}$) depend on pH; the data are shown in Table 1.

Usually, the reactivities of the **1** catalysts are less dependent on the substituents in the head component compared to the tail component.[8,19,27] The same holds for the acid-induced demetalations described here. The data in Figure 4B show that electron-donating or -withdrawing head groups do not affect the $k_{1,eff}$ much. As noted previously,[8,19,27] the reactivity of the unsubstituted Fe^{III}-TAML **1a** is higher than that expected in terms of the Hammett relationship,[28] whereas the rate constant ratio for

(26) Lewis, J. C. *Anal. Biochem.* **1966**, *14*, 495−496.
(27) Chanda, A.; Ryabov, A. D.; Mondal, S.; Alexandrova, L.; Ghosh, A.; Hangun-Balkir, Y.; Horwitz, C. P.; Collins, T. J. *Chem.−Eur. J.* **2006**, *12*, 9336−9345.
(28) Hammett, L. P. *Physical Organic Chemistry; Reaction Rates, Equilibria, and Mechanisms*, 2nd ed.; McGraw-Hill: New York, 1970.

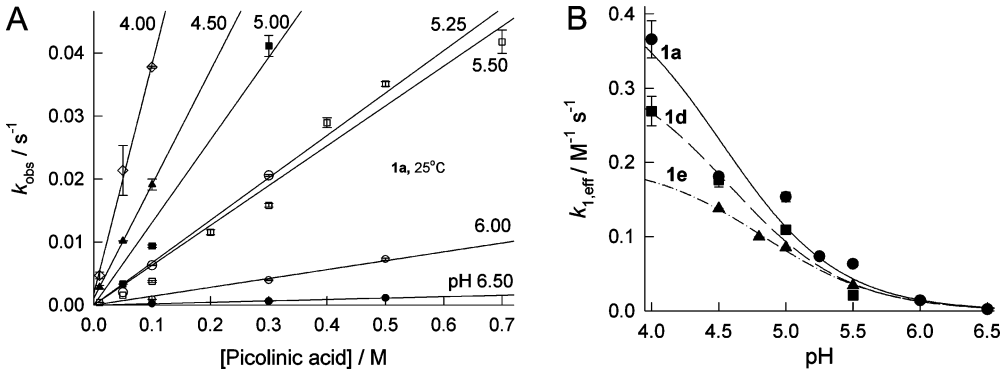

Figure 4. (A) Pseudo-first-order rate constants for demetalation of **1a** vs concentration of picolinic acid at different pHs and 25 °C. (B) Second-order rate constants $k_{1,eff}$ for demetalation of **1a** (●), **1d** (■), and **1e** (▲) as a function of pH. Solid lines are theoretical curves calculated using the best-fit values of the parameters of eq 1.

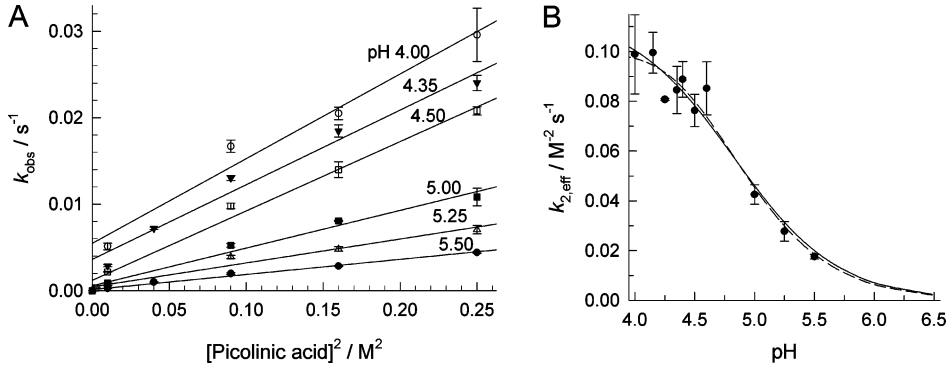

Figure 5. (A) Pseudo-first-order rate constants for the demetalation of **1b** at 65 °C against squared concentration of picolinic acid showing second order in the acid. (B) Third-order rate constants $k_{2,eff}$ for demetalation of **1b** as a function of pH. Solid and dashed lines are theoretical curves calculated using the best-fit values of parameters of eqs 1 and 12, respectively. See text for details.

electron-rich and -poor molecules **1d** and **1e**, respectively, is normal for an acid-driven process.

Complex **1b** is demetalated by picolinic acid (P2C) at 65 °C, but k_{obs} now depends in a second-order fashion on the picolinic acid concentration (Figure 5A).

$$k_{obs} = k_{0,eff} + k_{2,eff}\,[P2C]^2 \qquad (2)$$

Addition of the first order in ligand term $k_{1,eff}$[P2C] to eq 2 did not improve the fit. The third-order rate constants $k_{2,eff}$ (second order in ligand, first order in complex) calculated from the slopes of the linear plots in Figure 5A are shown as a function of pH in Figure 5B. Upon fitting the experimental data to eq 1, the parameters $a_1 = 0.116 \pm 0.007$ M^{-2} s^{-1} and $b_1 = (1.5 \pm 0.3)\times10^{-5}$ M were calculated. We will show below, however, that the picolinic acid case is exactly matched by the more elaborate definition of $k_{2,eff}$ given by eq 12.

But first, the difference in the reaction order in picolinic acid of one for **1a** and two for **1b** deserves consideration. If picolinic acid acts without kinetically meaningful binding to the iron(III) of **1** (there is no saturation in Figure 5A), the second order behavior could be rationalized by a self-association of picolinic acid to produce a more acidic dimer. Under such a hypothesis, the reaction order difference for **1a** and **1b** is hard to rationalize. An alternative mechanistic theory involves a first picolinic acid activating **1b** through binding with iron(III), with the second also binding to iron and engaging in the intramolecular proton delivery. In such a case, the demetalation by picolinic acid should also be accelerated by the addition of nicotinic or isonicotinic acids, which by themselves do not promote hydrolysis, but are capable of providing the axial pyridine acid that sets up the system for binding of the demetalating picolinic acid. Pyridine should produce the same effect. This expectation finds experimental support. Indeed, nicotinic acid (Figure 6) or pyridine (Figure 5S, Supporting Information) do speed up the demetalation of **1b** in the presence of picolinic acid. The observed hyperbolic dependence suggests a mechanism that involves a pre-equilibrium binding of two pyridine carboxylates to the Fe^{III} of **1b**, followed by the intramolecular proton transfer from the coordinated acid (Scheme 2). This option is supported by measurements of the binding constants for py and related ligands.

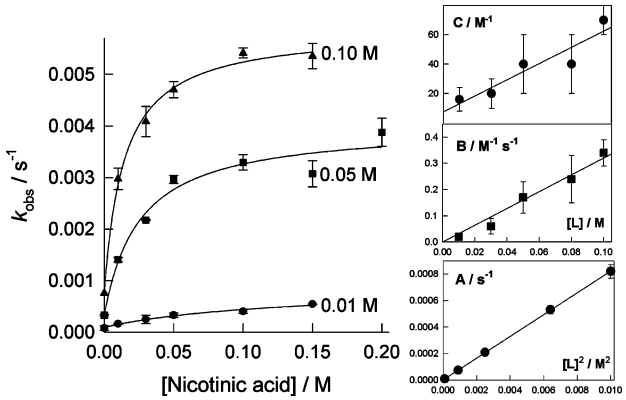

Figure 6. Effect of nicotinic acid on demetalation of **1b** in the presence of various concentrations of picolinic acid (0.01, 0.05, and 0.1 M) at pH 4.5 and 65 °C. Graphs in boxes on the right show anticipated dependencies of parameters *A*, *B*, and *C* of eq 9 on [P2C]^m ($m = 2$ for *A* and 1 for *B* and *C*). See text for more details.

Scheme 2. General Mechanism of Demetalation of **1** by Picolinic Acid Accounting for First (**1a**, in the Box) and Second (**1b**) Orders in the Acid

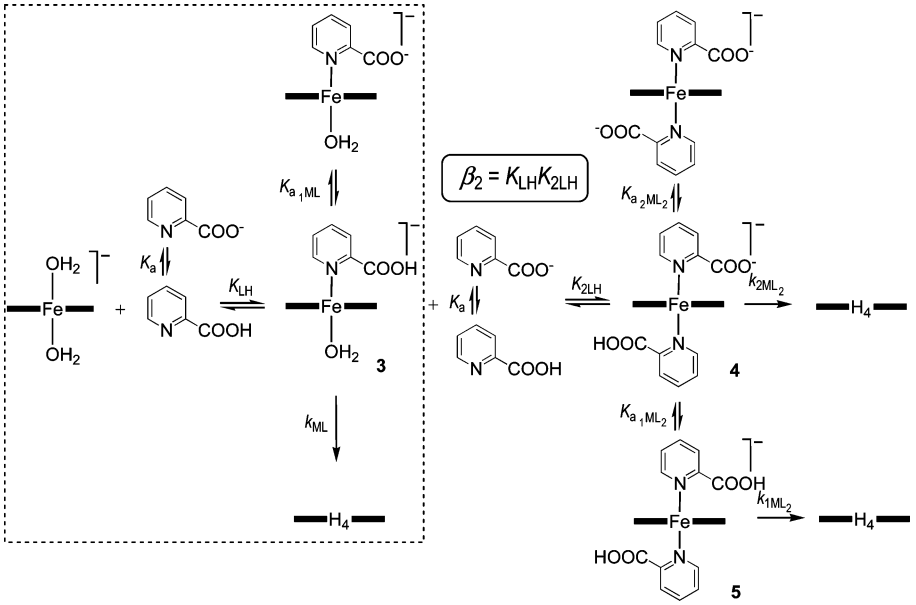

[a] Charge of the Fe^{III}-TAML complex is shown outside the bracket and localized charges are shown for the deprotonated pyridine carboxylates.

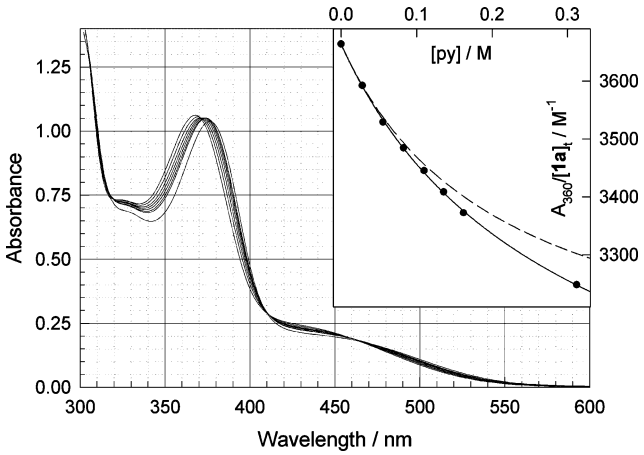

Figure 7. Spectral changes of **1a** (2.75×10^{-4} M) in the presence of pyridine: 0.1 M KPF_6, pH 6.3 and 25 °C. (Inset) Absorbance at 360 nm as a function of [py]; solid line is calculated curve using best-fit parameters of eq 4; broken line is a calculated curve with $K_{2L} = 0$ validating binding of the second axial ligand.

Thermodynamics of Axial Binding of Pyridines and Imidazoles to Iron(III) of 1. When pyridine is added to an aqueous solution of **1a**, the λ_{max} shifts from 368 to 376 nm at py concentrations 0−0.312 M, but there is no isosbestic point over the 300−600 nm range (Figure 7) suggesting the coexistence of at least three absorbing species. Assuming that they are as those in eqs 3, the py-induced spectral changes can be quantified using eq 4.

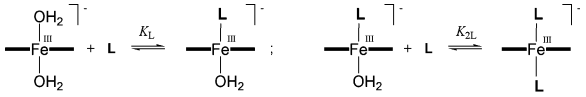

(3)

$$A = \frac{\epsilon_M + \epsilon_{ML}K_L[L] + \epsilon_{ML_2}K_LK_{2L}[L]^2}{1 + K_L[L] + K_LK_{2L}[L]^2}[M]_t \qquad (4)$$

Table 2. Equilibrium Constants of Fe^{III}-TAMLs **1** in Aqueous Solution at 25 °C, 0.1 M KPF_6

complex	L	pH	K_L/M^{-1}	K_{2L}/M^{-1}
1a	pyridine	5.0	4.7 ± 0.1	0.42 ± 0.03
1e			4.3 ± 0.3	could not be determined
1f			9.6 ± 1.0	could not be determined
1a	imidazole	6.3	69 ± 10	4.7 ± 4.5
1e			28.4 ± 0.8	16 ± 2
1f			24.1 ± 0.6	2.1 ± 0.1
1a	azide (N_3^-)	9.17	67 ± 6[a]	no evidence was obtained

[a] With 1.0 M $NaClO_4$ as a background electrolyte.

Here ϵ_M, ϵ_{ML}, and ϵ_{ML_2} are the respective extinction coefficients of all participants of eqs 3 and $[M]_t$ is the total concentration of **1**. The largest change in absorbance was observed at 360 nm and this wavelength was used for the calculation of K_L and K_{2L}. The fitting eq 4 to the experimental data with ϵ_M calculated at [py] = 0 (inset to Figure 7) gave K_L and K_{2L} (Table 2). The solid line in the Inset is a curve calculated using the best-fit values of ϵ_{ML}, ϵ_{ML_2}, K_L, and K_{2L}, while the broken line is the calculated prediction if $K_{2L} \approx 0$. The broken line deviates systematically from the experimental points giving evidence for the binding of the second py-type ligand. Similar behavior was observed for imidazole (Figure 8). The ascending curve (Inset) was fitted with eq 4 and the solid line was computed using the best-fit values of ϵ_{ML}, ϵ_{ML_2}, K_L, and K_{2L} (Table 2). The broken line indicates again that the second ligation is essential for a good fit.

Binding of pyridine and imidazole was investigated for complexes **1** with electron-withdrawing and -donating head groups, *viz.*, **1e** and **1f**. The equilibrium constants K_{2L} could not be determined reliably for pyridine binding to **1e,f**. The data in Table 2 reveal that imidazole is a better ligand for **1**. The relation $K_L > K_{2L}$ holds for both ligands, but the gap between K_L and K_{2L} is larger for pyridine. An opposite trend is observed for Fe^{II} and Fe^{III} porphyrins, for which only β_2 ($K_L \times K_{2L}$) is usually determined in water[29] and nonaqueous solutions.[30,31] In

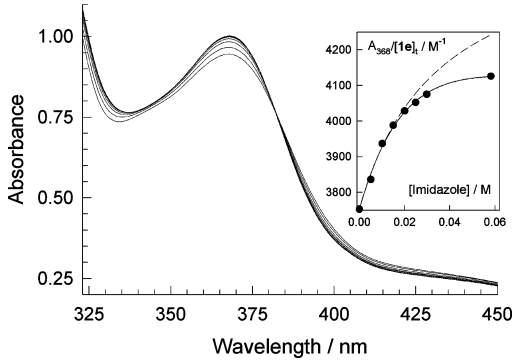

Figure 8. Spectral changes of **1e** (2.52×10^{-4} M) in the presence of imidazole: 0.1 M KPF_6, pH 6.3, 25 °C. (Inset) Absorbance at 368 nm as a function of [imidazole]; solid line is calculated curve using best-fit parameters of eq 4; broken line is a calculated curve with $K_{2L} = 0$ validating the binding of second axial ligand.

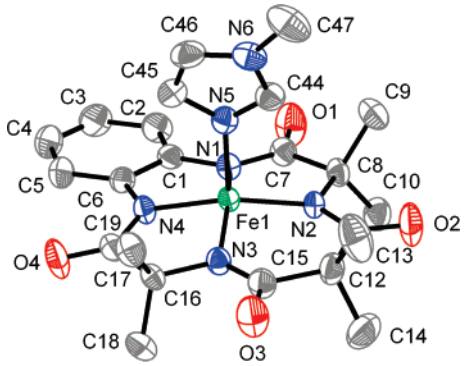

Figure 9. Molecular structure of the anionic part of **1a**-MeIm prepared from 1-methylimidazole (0.056 mmol) and $[Ph_4P]_2$[**1**-Cl] (0.0542 mmol) in 15 mL CH_2Cl_2. The solvent was allowed to evaporate leaving a light orange powder (92.5%). Displacement ellipsoids are drawn at the 50% probability level. H atoms omitted for clarity. Fe−N(1) 187.4(2) pm, Fe−N(2) 187.5(2) pm, Fe−N(3) 188.5(3) pm, Fe−N(4) 187.2(2) pm, Fe−N(5) 212.6(2) pm. DIAMOND release 3.1e, Crystal Impact GbR, Bonn, Germany.

water, only bis-ligated species are observed, which are however formed from iron-porphyrin dimers.[32,33]

The structure of the mono-ligated 1-methylimidazole (MeIm) adduct (**1a**−MeIm) was determined by X-ray crystallography (Figure 9). The imidazole plane is practically parallel to a plane through atoms Fe1, N2 and N4 (dihedral angle 11.2(2)°). If a similar geometry holds for the coordinated picolinic acid, its carboxylic group should be in the closest proximity to the Fe−N amide bond that finally will be cleaved—the geometric feature appropriate for intramolecular catalysis.

The data in Figures 7 and 8 indicate that species **3** and **4** in Scheme 2 are plausible intermediates in the demetalation of **1a** and **1b**, respectively. Picolinic acid binds to the axial site of Fe^{III} and then delivers the carboxylic proton to a Fe−N bond. This is more difficult in the case of **1b** where the amidato-N donor atoms are less basic. Therefore, the second py ligand may increase the electron density at the Fe−N bonds and it may also affect the location of the iron atom with respect to the plane of the four amidato ligands in a manner that favors the demetalation. It is significant that the picolinic acid α-carboxylic

Scheme 3. Stoichiometric Mechanism of Demetalation of Robust Fe^{III}-TAMLs Such as **1b** by Picolinic Acid (L) in the Presence of Other Pyridines (P)[a]

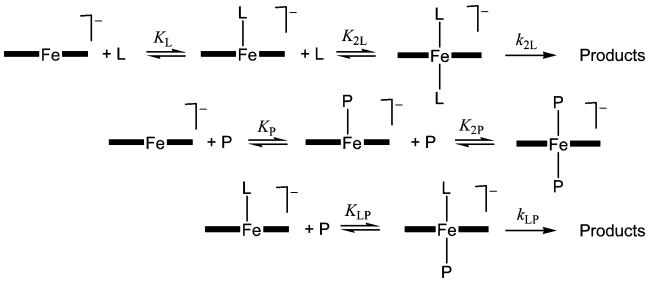

[a] Axial aqua ligands are omitted for clarity.

group is clearly not essential for this second pyridine ligand because both py and nicotinic also accelerate the demetalation (Figure 6). This data is quantifiable in terms of the mechanism in Scheme 3. The reactive intermediates for robust **1b** is the diaxially coordinated species, one of the two ligands being picolinic acid (L).

Scheme 3 leads to eq 5 for the pseudo-first-order rate constant for demetalation of **1b** at a given pH when the concentration of total iron (M_t) is much less than that of L and P.

$$k_{obs} = \frac{k_{2L}K_LK_{2L}[L]^2 + k_{LP}K_LK_{LP}[L][P]}{1 + K_L[L] + K_P[P] + K_LK_{2L}[L]^2 + K_PK_{2P}[P]^2 + K_LK_{LP}[L][P]} \quad (5)$$

In the absence of added P, eq 5 transforms into eq 6.

$$k_{obs} = \frac{k_{2L}K_LK_{2L}[L]^2}{1 + K_L[L] + K_LK_{2L}[L]^2} \quad (6)$$

The experimentally observed second order in L (eq 2) implies that $1 \gg K_L[L] + K_LK_{2L}[L]^2$ and $k_{2,eff} = k_LK_LK_{2L}$. Therefore, in the presence of P, eq 5 appears in the form

$$k_{obs} = \frac{k_{2L}K_LK_{2L}[L]^2 + k_{LP}K_LK_{LP}[L][P]}{1 + K_P[P] + K_PK_{2P}[P]^2 + K_LK_{LP}[L][P]} \quad (7)$$

The dependence of k_{obs} on [P] is hyperbolic (Figure 6) and hence the term $K_PK_{2P}[P]^2$ in the denominator is negligible. Consequently

$$k_{obs} = \frac{k_{2L}K_LK_{2L}[L]^2 + k_{LP}K_LK_{LP}[L][P]}{1 + (K_P + K_LK_{LP}[L])[P]} \quad (8)$$

At constant L, the dependence of k_{obs} on [P] appears as

$$k_{obs} = \frac{A + B[P]}{1 + C[P]} \quad (9)$$

Here $A = k_{2L}K_LK_{2L}[L]$,^{2} $B = k_{LP}K_LK_{LP}[L]$, and $C = K_P + K_LK_{2L}[L]$. Parameters *A*, *B*, and *C* of eq 9 were obtained by fitting the data in Figure 6 to eq 9 at five concentrations of picolinic acid. Both *B* and *C* should be linear functions of [L], whereas *A* should be proportional to [L].^{2} The graphs in the small boxes of Figure 6 show that such dependencies hold. The plots *A* and *B* versus [L] and [L],^{2} respectively, go through the origin. An intercept of the plot *C* against [L], which should

(29) Fleischer, E. B.; Fine, D. A. *Inorg. Chim. Acta* **1978**, *29*, 267−271.
(30) Coyle, C. L.; Rafson, P. A.; Abbott, E. H. *Inorg. Chem.* **1973**, *12*, 2007−2010.
(31) Nesset, M. J. M.; Shokhirev, N. V.; Enemark, P. D.; Jacobson, S. E.; Walker, F. A. *Inorg. Chem.* **1996**, *35*, 5188−5200.
(32) Shack, J.; Clark, W. M. *J. Biol. Chem.* **1947**, *171*, 143−187.
(33) Cowgill, R. W.; Clark, W. M. *J. Biol. Chem.* **1952**, *198*, 33−61.

equal K_P, is close to 8 M^{-1} and falls into the range of K_L reported in Table 2.

Binding of Azide and Estimation of the Rate of Exchange of Water in Coordination Sphere of 1a. Azide ion does not catalyze the demetalation, but the interaction of **1** with azide is accompanied by a significant optical change. Therefore, it has been used for ligand equilibrium binding studies. Absorbance values at several different wavelengths were measured as a function of azide concentration (Figure 6S, Supporting Information, gives sample spectra). The formation constant of the complex was determined by fitting the experimental data to eq 4, which gave $K_{2L} = 0$ within experimental error. The binding of azide occurs too fast even for measuring by a stopped-flow technique. However, the data was used to estimate the rate constant of water exchange in the first coordination sphere of **1a** (see Supporting Information). The lower limit of 1.9×10^5 s^{-1} (25.0 °C, pH 9.17, 1.0 M $NaClO_4$) is closer to rate constants for exchange in the aqua Fe^{II} cation than in Fe^{III}.[34] This feature of **1** was previously highlighted to account for the unique reactivity of **1** toward O_2 in aprotic solvents.[35]

Second Tier Kinetic Analysis. Equation 1 corresponds to a kinetic model shown in Scheme 1. The generalized mechanism is shown in Scheme 2. Its boxed part gives kinetic eq 10 valid at pH 4−6.5 because [P2C] ≫[**1a**] and the pK_a of the pyridine nitrogen of P2C equals 1.60.[36]

$$k_{obs} = \frac{k_{ML}K_{LH}L_t[H^+]}{(K_a + [H^+]) + K_{LH}L_t[H^+] + K_{a1ML}K_{LH}L_t} \quad (10)$$

First-order behavior in L_t (Figure 4A) is realized when $(K_a + [H^+]) \gg K_{LH}L_t[H^+] + K_{a_{1ML}}K_{LH}L_t$)[37] and eq 10 simplifies to eq 1 with $a_1 = k_{ML}K_{LH}$ and $b_1 = K_a$. Thus, the enthalpy and entropy of activation of 47 kJ mol^{-1} and −143 J K^{-1} mol^{-1}, respectively (Table 1), correspond to the product $k_{ML}K_{LH}$. Provided that the temperature dependence of K_{LH} is small ($\Delta H°_{LH} \approx 0$),[38] $\Delta H^{\neq}$ should reflect the proton transfer at the Fe−N bond[39] and this value is normal for an associative process.[25] The K_a for $H_2PO_4^-$ increases with temperature and then decreases (Table 1), and this fact has previously been documented.[40,41] Given the assumption that $k_{ML} \approx 0$, the entire Scheme 2 leads to eq 11 ($\beta_2 = K_{LH}K_{2LH}$).

$$k_{obs} = \frac{(k_{1ML2}[H^+]^2 + k_{2ML2}K_{a1ML2}[H^+])\beta_2 L_t^2}{(K_a + [H^+])^2 + ([H^+]^2 + K_{a1ML2}[H^+] + K_{a1ML2}K_{a2ML2})\beta_2 L_t^2} \quad (11)$$

The second kinetic order in L_t indicates that $(K_a + [H^+])^2 \gg ([H^+]^2 + K_{a1ML2}[H^+] + K_{a1ML2}K_{a2ML2})\beta_2 L_t^2$ and the expression for $k_{2,eff}$ appears as eq 12 where $a_3 = k_{1ML2}\beta_2$, $b_3 = K_{2ML2}K_{a1ML2}\beta_2$, and $c_3 = K_a$. The dashed line in Figure 5B, plotted using the best fit values of a_3, b_3, and c_3, has a small advantage over the solid line calculated using eq 1 (see Supporting Information for an expanded kinetic analysis).

$$k_{2,eff} = \frac{a_3[H^+]^2 + b_3[H^+]}{(c_3 + [H^+])^2} \quad (12)$$

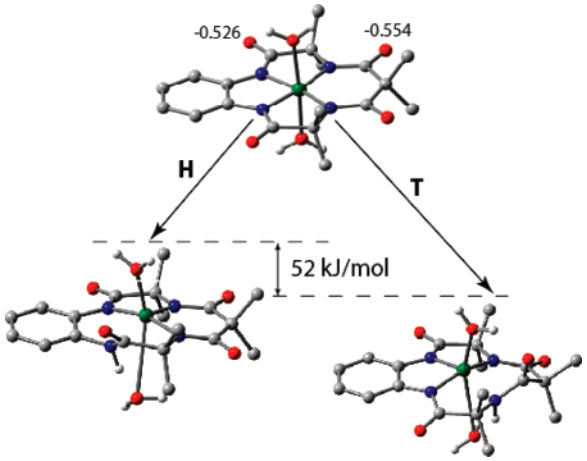

Figure 10. DFT calculated Mulliken charges of tail and head amide oxygens (top structure) of diaqua form of **1a** and relative energies of the intermediates of demetalation with cleaved Fe−N bonds in the head (**H**) and tail part (**T**) of the molecule (bottom structures). Hydrogens attached to carbon atoms are not shown for clarity.

Mechanistically Relevant DFT Analysis of Fe^{III}-TAMLs. DFT calculations combined with kinetic and structural data are particularly beneficial. Our DFT studies were inspired by a variety of relevant kinetic and X-ray results.[19] The dissociation of Fe^{III} from **1** is a subject of both specific acid and acidic buffer ion induced catalysis. The former dominates at pH < 3 and includes first- and third-order pathways (in H^+).[19] The buffer ion promoted dissociation is manifested at pH > 4 and cannot be ignored until pH ≈ 8 with the active buffer ions studied here. The third-order pathway k_3 has been interpreted in terms of pre-equilibrium protonation of two amide oxygens followed by the rate-limiting cleavage of Fe−N bond by the third proton. Substituents at the tail part of **1** have been shown to affect the first and third-order pathways in a 10^5- and 10^{11}-fold ranges, respectively, and this was taken as evidence that the rate-limiting cleavage of the Fe−N bond occurs at the tail part.

DFT studies made in vacuum for the six-coordinated diaqua species (**1a**) in Figure 10 support these conclusions. Though the calculated negative charge density at the amide nitrogens is the highest, the amide oxygens are more prone to protonation because they are more exposed to the solvent. For **1a**, the Mulliken charges on the amide oxygens equal −0.554 and −0.526 for the tail and head, respectively (Figure 10). The difference amounts to a substantial determiner of reactivity as can be deduced by comparing the Mulliken charges at the tail amido oxygens of **1a** (−0.554) and **1c** (−0.491), *i.e.* complexes with drastically different reactivities.[19] DFT calculations were used to explore the energetics of protonation and these studies indicate that the proton-induced cleavage of the Fe−N_{TAIL} bond is more exergonic than that of the Fe−N_{HEAD} bond (Figure 10). The energy difference for the diaqua form of **1a** equals 52 kJ

(34) Cusanelli, A.; Frey, U.; Richens, D. T.; Merbach, A. E. *J. Am. Chem. Soc.* **1996**, *118*, 5265−5271.
(35) Ghosh, A.; Tiago de Oliveria, F.; Toshihiro Yano, T.; Nishioka, T.; Beach, E. S.; Kinoshita, I.; Münck, E.; Ryabov, A. D.; Horwits, C. P.; Collins, T. J. *J. Am. Chem. Soc.* **2005**, *127*, 2505−2513.
(36) Jellinek, H. H. G.; Urwin, J. R. *J. Phys. Chem.* **1954**, *58*, 548−550.
(37) It is interesting to note that eq 10 indicates that a reaction rate is determined by the pK_a of free and coordinated ligand in the case of weak or "saturative" binding, respectively.
(38) Smith, R. M.; Martell, A. E. *Critical Stability Constants*; Plenum Press: New York and London, 1975.
(39) The observed enthalpy of activation for $a_1 = k_{ML}K_{LH}$ equals $\Delta H^{\neq}_{obs} = (\Delta H^{\neq}_{kML} + \Delta H°_{KLH})$. Since $\Delta H°_{KLH} \approx 0$, $\Delta H^{\neq}_{obs} = \Delta H^{\neq}_{kML}$.
(40) Nims, L. F. *J. Am. Chem. Soc.* **1933**, *55*, 1946−1951.
(41) Grzybowski, A. K. *J. Phys. Chem.* **1958**, *62*, 555−559.

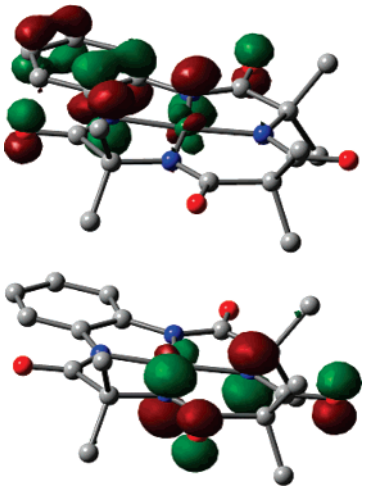

Figure 11. HOMO (top) and second highest occupied molecular orbital, sHOMO (bottom) of **1a** predicted by DFT calculations. Hydrogen atoms and axial oxygens are not shown for clarity.

mol^{-1}. This may pull down the free energy of activation in favor of the T-pathway.

Although Mulliken charges are helpful for mechanistic choices, frontier molecular orbitals of reacting molecules are more relevant.[42,43] All the molecular orbitals of the diaqua form of **1a** were calculated. The HOMO and the second highest occupied MO (sHOMO) are shown in Figure 11. In an earlier study we have shown that the HOMO is primarily a "redox active" orbital. It is noticeably delocalized over the aromatic ring and two adjacent amide moieties.[21] Therefore a proton attack at this orbital is difficult to perceive. On the other hand, the electronic density of the sHOMO is much less diffuse and *solely* localized at the nitrogen and oxygen atoms of the tail amide fragment (Figure 11). The sHOMO is thus an ideal target for the protonation followed by Fe−N bond cleavage and demetalation. Though the overall energy of the sHOMO is slightly lower than that of HOMO, this orbital should be more susceptible to the electrophilic proton attack *via* both the specific acid and the buffer ion coordination/protonolysis mechanisms. Also, the sHOMO is well organized for both peripheral pre-equilibrium protonation and direct attack at the Fe−N bond. Note that solvation may influence the relative energies of molecular orbitals.

Conclusion

Acid-catalyzed demetalation of Fe^{III}-TAMLs **1** begins when a Brønsted acid coordinates to the iron(III) and delivers its proton in an intramolecular fashion via a favored six-membered ring to the proximity of an Fe−N bond resulting in its cleavage. This mechanism is consistent with the fact that picolinic acid catalyzes the demetalation, but nicotinic and isonicotinic acids do not. Acids such as $H_2PO_4^-$, HSO_3^-, or CH_3COOH have suitable structures to coordinate to the iron of Fe^{III}-TAMLs *via* their O-atoms and deliver their protons intramolecularly to the vicinity of an Fe−N bond to promote protonolysis. The mechanism of demetalation disclosed in this work shows how buffer components can be chosen based on their structures and acidities so that they will be inactive in the demetalation in the vicinity of neutral pH. In characterizing the reaction, it is important to note that it should not be labeled as a case of specific acid catalysis, because the free proton is not implicated, and while we do not object to the general acid catalysis label, it is important to note that only one of all the proton sources in any given solution contributes to driving the hydrolyses and, most unusually, the catalysis is also predicated upon precoordination of the buffer ion. We have considered giving the reaction type another name, but it is sufficiently specialized that a simple name that accurately captures what is going on is not obvious. Preferably, buffers chosen to avoid demetalation should not have pK_a's in the range 4−8, but if there is a particular advantage for any such buffer, the proton-bearing buffer ion should not have a structure that enables it to bind to the iron(III) of **1** and deliver a proton in an intramolecular fashion to a coordinated amidato-N atom, i.e., avoid 6- and probably also 5-membered rings for proton delivery, Scheme 1. The knowledge developed in this study is especially valuable for avoiding unfavorable catalyst degradation processes in functioning Fe^{III}-TAML activator systems as well as for storing Fe^{III}-TAML catalyst solutions. It also indicates another viable approach for deactivating certain Fe^{III}-TAML activators to add to the well-parametrized oxidative deactivation routes,[27] if such is needed, after they have been used in a process and before in an effluent stream would be released to the environment.

Experimental Section

Instrumentation. Kinetic and spectrophotometric measurements were carried out on Hewlett-Packard Diode Array spectrophotometers (models 8452A and 8453) or a Perkin-Elmer Lambda 900 UV/vis-NIR spectrophotometer equipped with a thermostated cell holder and automatic 8-cell positioner. ^{1}H NMR data were obtained at 300 K with a Bruker Avance DMX-500 (operating at 500.13 MHz) equipped with a Multinuclear Inverse Broadband (BBI) probe (5 mm sample diameter), using the built-in pulse "zg". X-band (9.62 GHz)

Materials. Fe^{III}-TAML complexes **1a**−**f** were synthesized at Carnegie Mellon University by published methods.[44,45] All other reagents and solvents (at least ACS reagent grade) were obtained from commercial sources (Aldrich, Fisher, Across, Fluka) and used as received or, if necessary, after purification as described elsewhere.[46]

Products of Demetalation of 1a. Compound **1a** (250 mg) was dissolved in 5 mL of 0.5 M phosphate pH 7 buffer. The color of the buffer solution became noticeably lighter within minutes. The solution was kept overnight at room temperature. A white precipitate formed was separated and washed with acetone. No extensive drying was applied. A few milligrams were added to methanol-d_4. The mixture was filtered through glass wool and introduced into the NMR tube. 16 scans were collected. Processing was carried out using SpinWorks software version 2.5 (Kirk Marat, http://www.umanitoba.ca/chemistry/nmr/spinworks).

Kinetic and Equilibrium Measurements. Stock solutions of complexes **1** (*ca.* 0.005 M) were prepared in acetonitrile solvent. Kinetic and equilibrium measurements were carried in both buffered and non-buffered (in the presence of 0.1 M KPF_6) doubly distilled or HPLC grade water. The progress of demetalation was monitored by following the absorbance decrease at 365 nm. Concentrations of **1** in 1 cm plastic UV/vis cells (Fischer, # 14−385-938) were kept around 4.5×10^{-5}

(42) Fukui, K. *Angew. Chem.* **1982**, *94*, 852−861.
(43) Woodward, R. B.; Hoffmann, R. *The Conservation of Orbital Symmetry*; Academic Press: New York, 1970.
(44) Website http://www.chem.cmu.edu/groups/collins/awardpatpub/patents/index.html.
(45) Ghosh, A. *Design, Synthesis and Mechanistic Studies of Iron-TAML Catalytic Activators of Hydrogen Peroxide and a New Activation Chemistry of Dioxygen by Iron*; Ph.D. Thesis, Department of Chemistry, Carnegie Mellon University, Pittsburgh, PA, 2004.
(46) Perrin, D. D.; Armarego, W. L. F. *Purification of Laboratory Chemicals*, 3rd ed.; Pergamon Press: Oxford and New York, 1988.

The ionic strength was not kept constant in all kinetic runs because neutral salts do not noticeably influence the rate of demetalation. Pseudo-first-order rate constants (k_{obs}) were calculated by fitting the absorbance (A) versus time (t) traces to the equation $A = A_\infty - (A_\infty - A_o) \times \exp(-k_{obs} \times t)$ where A_o and A_∞ are absorbances at times 0 and ∞, respectively. Good first-order holds for at least 4−5 lives. All k_{obs} reported are mean values of at least three determinations. Calculations were carried out using a Sigma Plot 7.00 package.

DFT Calculations. Density functional calculations were performed using Becke's three parameter hybrid functional (B3LYP) provided by the Gaussian 03 (release B.05) software package.[47] The basis set 6-31G was used for geometry optimizations and Mulliken charge analysis. All calculations were carried out in vacuum (in the absence of any solvent). Mulliken population analysis was employed to monitor electron distribution. The SCF calculations were terminated upon reaching tight convergence criteria (10^{-6} root-mean-square deviation in the density matrix and 10^{-8} atomic unit maximum deviation in energy).

Single-Crystal X-Ray Characterization of (1a·MeIm). Single crystals of **1a**-MeIm were obtained from CH_2Cl_2/pentane. Anal. Found C 66.59 H 5.71, N 9.91. Calcld. for $C_{47}H_{51}N_6PO_4Fe{\cdot}CH_2Cl_2$. C 66.59, H 5.68, N 9.82%. $C_{47}H_{48}FeN_6O_4P$, $M_r = 847.8$, monoclinic, $P2_1$, orange, $a = 9.9865(8)$ Å, $b = 15.9335(8)$ Å, $c = 13.252(2)$ Å, $\beta = 95.115(9)°$, $T = 299$ K, $Z = 2$, $R_1 = 0.040$, w$R_2 = 0.092$, GOF = 1.11, Flack parameter $x = -0.012(13)$. Data collection on a Bruker-Nonius KappaCCD (Mo Kα radiation), structure solution with direct methods, structure refinement on F^2 with anisotropic thermal parameters for all non-H atoms. H atoms were placed at calculated positions and refined using a riding model.

(47) Frisch, M. J.; et al. *Gaussian 03*, revision B.05; Gaussian, Inc.: Wallingford, CT, 2004.

Acknowledgment. Operating support is acknowledged from the Heinz Endowments (T.J.C.), the Eden Hall Foundation (T.J.C.), the Institute for Green Oxidation Chemistry (T.J.C.), the Environmental Protection Agency (grant RD 83 to T.J.C.), and the Hungarian Science Foundation OTKA (F049498 to G.L. and I.F.). V.P. thanks the Howard Hughes Medical Institute for an Undergraduate Research Grant. E.S.B. is a National Science Foundation Graduate Research Fellow and is grateful to the AATCC Foundation Student Research Support Grant Program for the award of additional support. We acknowledge the National Science Foundation for purchasing the NMR spectrometer of the Department of Chemistry at Carnegie Mellon University (CHE-0130903). The Swedish Research Council (V.R.) is acknowledged for providing funding for the single-crystal diffractometer.

Supporting Information Available: Graphs with rate constants for demetalation of **1a** in the presence of sulfite, acetate, malonate, pyridine and picolinic acid (for **1b**); the Brønsted plot; spectral changes on complexation of **1a** with azide. Method for the estimation of the lower limit for the water exchange rate constant of **1a**; X-ray crystallographic data. Complete ref 47. This material is available free of charge via the Internet at http://pubs.acs.org.

JA7106383